TEL-AVIV UNIVERSITY
GEORGE S. WISE FACULTY OF LIFE SCIENCES
GRADUATE SCHOOL

Independent and cooperative motions of the Kv1.2 channel: Voltage-sensing and gating

Thesis submitted towards the M.Sc. degree in Biochemistry
at Tel-Aviv University

by
Adva Yeheskel

The research was performed in the

Department of Biochemistry

under the supervision of

Prof. Nir Ben-Tal

Date: January 2009

Thanks

First I would like to thank Prof. Nir Ben-Tal and Prof. Turkan Haliloglu for their guidance and for allowing me to learn and do science.

I would like to thank Ugur Emekli for the help with the HingeProt web-server and Guy Nimrod for helpful discussions.

I also thank Prof. Diane Papazian, Dr. Vladimir Yarov-Yarovoy and Prof. Roderick MacKinnon for the coordinates of their Kv structure models.

List of contents

Abstract

Voltage-gated potassium (Kv) channels, such as Kv1.2, are involved in the generation and propagation of action potentials. The Kv channel is a homotetramer; each monomer is composed of a voltage-sensing domain (VSD) and a pore domain (PD). To further our understanding on how the conformational changes in the domains facilitate the open/close transition of the pore, we analyzed the fluctuations of a model structure of Kv1.2 using the Gaussian Network Model (GNM) and Anisotropic Network Model (ANM). GNM was used to identify hinge regions and rigid elements of the structure, and the dynamic coupling between them, and ANM was used to predict the directions of movements of the elements. The analysis decomposes the motion into a set of discrete modes, and it is often possible to associate the slowest ones with biological functions. Here, the voltage-sensing and gating motions were found to be described by two groups of modes. The analysis suggested a network of coupled fluctuations of eight rigid structural units coordinated with seven hinges. For the most part, the network is composed of amino acids that have been known to be involved in conformational changes associated with the transition between active and inactive states of the channel, and/or to be sensitive to mutations. The results suggested coupling between the motion of the VSD and the selectivity filter of the PD, in accordance with recent empirical data. The coupling, which is suggestive of functional relations between these remote regions, was not observed in the isolated monomer, indicating its allosteric nature. There are no direct contacts between the VSDs of the four subunits, and the contacts between these and the PDs are loose, suggesting that they are capable of functioning independently. Indeed, they manifest many inherent fluctuations that are decoupled from the rest of the structure. In general, the analysis suggests that the two domains contribute to the channel function both individually and cooperatively.

Introduction

The voltage gated potassium (Kv) channel aids in the repolarization phase of action potentials; therefore it is very important for the proper communication between neurons and other excitable cells. These channels are located in the brain, ear and heart. Mutations of amino acids in Kv channels cause episodic ataxia syndromes, epilepsy, deafness, long QT syndrome and other disorders (1). Recently, two new features of Kv channels were discovered. Kv channels were shown to be affected by viral products in Human immunodeficiency virus type-1 (HIV-1)-associated dementia (2). Furthermore, a functional connection between *Shaker*, a Kv channel in *Drosophila*, and a sleep-promoting factor was shown (3).

Several X-ray structures of Kv channels are available. MacKinnon's group solved the structure of rat Kv1.2 in its open state (4, 5). Yarov-Yarovoy (6, 7) created model structures with the VSD loops that were missing in MacKinnon's structure (5). MacKinnon's group also solved the structure of a chimera protein Kv1.2 with the S3-S4 paddle from Kv2.1 (8) and the structure of KvAP, a homologous protein from archea, and modeled it in a lipid membrane (9); this structure was also modeled by Yarov-Yarovoy (7). The PD is similar in all the structures and the differences are mainly in the sensor domain. An elaborated description of all X-ray and modeled structures of Kv channels which were analyzed here is available in Appendix 1.

Kv channels are composed of four identical monomers, each containing two domains (Fig. 1b): the voltage-sensing domain (VSD) and the pore domain (PD). The VSD includes helices S1-S4. The PD includes helices S5-S6, connected by a re-entrant loop, which is involved in ion selectivity. It is thought that voltage changes in the membrane affect the pore opening through four conserved arginine residues that are located in helix S4 (R294, R297, R300, R303) (10-14). Mutations of arginine residues in the S4 helix allow the nonselective conductance of various cations, a phenomenon called "omega currents". Mutating specific residues in the S4 helix causes a leak of protons (15). Recently it has been shown that the omega currents are associated with four "omega pores" per K-channel (16).

The VSD is also found in calcium (Cav) and sodium (Nav) channels (17). The same voltage sensor also controls a phosphatase activity in the ascidian VSD protein Ci-VSP (18-20). Kohout et al suggested that the protein works as a monomer, and that it uses a multi-step rearrangement in its activity, similar to the VSD of voltage gated ion channels (21). Recently, a voltage gated proton channel (VSOP or Hv) was discovered which comprises the VSD alone (22). This protein shares about 30% sequence identity with the Kv1.2 VSD. They are also believed to share the same fold. Alabi et al transferred the S3-S4 paddle from VSOP and Ci-VSP (one from each) into Kv2.1 and showed that the chimera proteins are functional (23). It suggests that the voltage-sensing mechanism is conserved between these remotely homologous proteins. The fact that the VSD preserves its motions in various structural architectures supports the idea that it serves as a modular structural unit.

Three main models have been proposed for voltage sensing in Kv channels and the movement of the S4 helix in particular. The transporter model suggests that during activation, the S4 arginines are moving from crevice with intracellular solution to crevice with extracellular solution. The motion of the S4 helix involves rotation and tilting. In addition motions within the VSD change the shape of the crevices (24-26). In the helical screw model, the S4 helix changes its location in the plane of the membrane and rotates (27, 28). This motion was suggested to be induced by a gating pore, also called omega pore, which insulates the S4 helix from the membrane (29-31). In the paddle model, proposed based on the KvAP structure, S3 and S4 form a helical hairpin that moves across the membrane as a unit. This model suggests that the paddle is exposed to the lipid in both states (4, 32).

Two previous studies, using normal mode analyses of K-channels, investigated the global motions of the pore domain (33, 34). The present work is an extension of the previous two, where the main goal is to identify communication between the voltage sensor and the pore. Searching for large conformational changes in such model structures by atomistic simulations is computationally demanding, and normal mode analysis, using elastic network models, provides an alternative. These coarse grained models might not substitute full atom simulations but analysis of the fluctuation modes often provides mechanistic insight on protein motion and its implication for function (35).

Here, we used GNM (36, 37) and ANM (38, 39) to carry out an elaborated analysis on the structural fluctuations of the Kv1.2 model structure. The combined analysis of GNM and ANM allowed the prediction of the hinge regions, the rigid structural elements that connect them, and the cooperative movements that may be involved in the channel's function.

Methods

Structure

We used an existing model structure of the rat Kv1.2 channel in an open conformation (7). The structure was built using ROSETTA (7) based on the incomplete X-ray structure of reference (5) (PDB 2A79). The channel is a homotetramer and each monomer has 260 residues in the membrane. The monomer contains two transmembrane domains: VSD and PD (Fig. 1b), and a tetramerization domain (T1) which is intracellular. The VSD is composed of four helical transmembranal segments: S1 (A162-Q193), S2 (D220-C244), S3 (N253-K277) and S4 (G284-S311). The PD is composed of two helical transmembranal segments (S5: M325-Q350 and S6: I385-T421) connected by a reentrant loop (A351-T384). The VSD and PD are connected by a short helical segment (S4-S5 linker; residues K312-S324). In addition, each monomer has 161 residues and 78 residues in its N- and C-termini that were deleted from the structure. The analysis was preformed on the transmembrane domains; the T1 domain was deleted. GNM calculations were also conducted for several other 3D structures (*Appendix 2*).

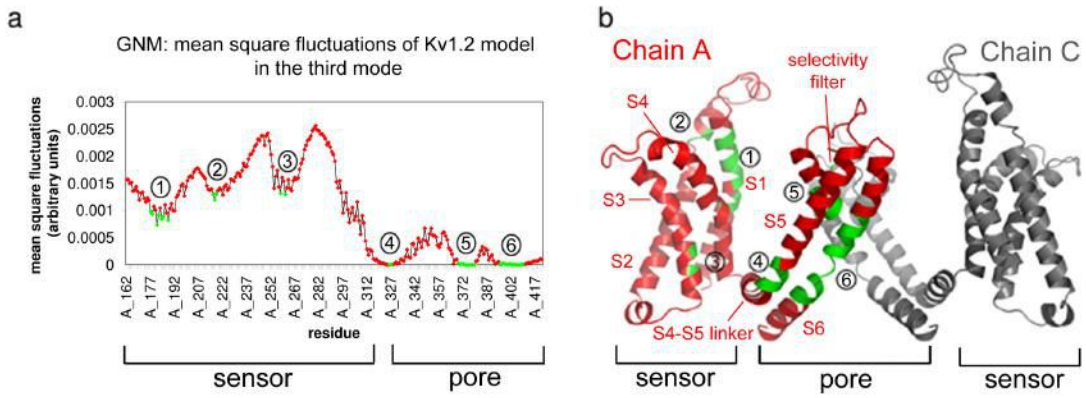

Figure 1: Identification of hinges. (a) Mean square fluctuations of the third mode. The minima, corresponding to the hinges, are labeled in green and marked from 1-through-6. (b) Two juxtaposed monomers of Kv1.2's model structure (7): Chain A (red) and chain C (gray). Transmembrane helices S1-through-S6 are marked in red and the six hinge-regions (green) are marked using the grey encircled numbers. The figure was prepared using Pymol (http://www.pymol.org).

Elastic Network Models

We analyzed the Kv1.2 model structure through elastic network models, namely GNM (36, 37) and ANM (38, 39). In these elastic models, the protein structure, simplified into C-alpha atoms, is treated as an elastic network of residues connected by hookean springs within a cutoff distance. The fluctuations can be decomposed into N-1 and 3N-6 normal modes in GNM and ANM, respectively, and thus the real motion could be expressed as linear combinations of the fluctuations in these normal modes. The contribution of each motion is scaled with the inverse frequency of that mode. The slowest modes thus contribute most to the predicted fluctuations. Often, the slowest modes are related to motion that is associated with biological functions of the macromolecule (35).

Of the two elastic models, GNM is known as more robust in the mean square fluctuations. Thus, it was used here to predict the relative magnitudes of fluctuations of the amino acids in order to identify hinge regions. The correlation between the fluctuations in the slowest modes of motion was used to predict the cooperation between the rigid structural elements. The eight slowest modes, further decomposed into the first three and the next five, were chosen for the analysis based on the distribution of the eigenvalues (see *Results*).

ANM was then used to predict the directions of motions and to generate the conformations that describe the fluctuations in 3D in the corresponding modes. The mean square fluctuations by GNM and ANM were compared to find the corresponding modes (35, 39).

The calculations were conducted with distance cutoffs of 10 and 15 Å for the GNM and ANM calculations, respectively. The HingeProt webserver ((39); http://www.prc.boun.edu.tr/appserv/prc/HingeProt3/index.html) was utilized in the calculations together with *in house* GNM/ANM programs. More details about the GNM and ANM models are provided in Appendix 3.

Evolutionary conservation

The degree of evolutionary conservation of each residue was calculated using the ConSeq web-server ((40); http://conseq.bioinfo.tau.ac.il/). We used rat Kv1.2 as the input

sequence. A multiple sequence alignment of homologous proteins was built by MUSCLE (41) using 125 homologous sequences from the SWISSPROT database (42). The alignment, available in http://ibis.tau.ac.il/wiki/nir_bental/index.php/Adva, contains the nine voltage gated potassium channels sub-families as well as calcium activated potassium channels and other voltage gated cation channels. The conservation scores of the amino acid positions were estimated using an empirical Bayesian inference method (43). The results were color-coded on the sequence using the key in Figure 2. The multiple sequence alignment was also used to identify polymorphism between Kv channels within positions which are located close to hinge points.

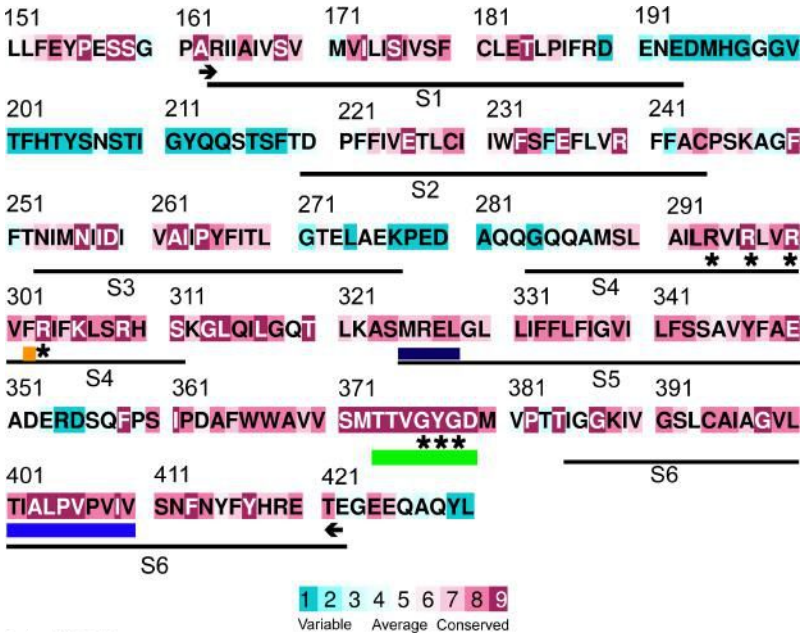

Figure 2: ConSeq analysis of rat Kv1.2. The sequence is colored using the conservation scale at the bottom: variable residues are in turquoise, conserved residues are in burgundy. The two arrows near the N- and C- termini mark the boundaries of the structure, and the locations of the S1-to-S6 helices are indicated. The S4 arginines and selectivity filter are marked by asterisks. Important hinge points and areas with restricted mobility are marked by colored rectangles: 302 in orange (the S4 helix), 325-328 in dark blue (the S5 helix), 373-379 in green (the pore loop) and 402-410 in blue (the S6 helix). The transmembrane segments S1-through-S6 are conserved and show a helical conservation pattern, as anticipated. The loops between the helices of the VSD (S1-S4) are variable. Most of the hinge regions are conserved.

Results

First, we describe the global motions of the channel suggested by the GNM and ANM modes. Next, we focus on the correlations between the fluctuations of specific rigid elements and explore the coupling between the motions within and between the two domains.

a. Hinges and rigid elements

We ranked the modes from the slowest to the fastest and looked at the distribution of their eigenvalues (eigenfrequencies). We used the first eight modes, which appeared as sufficient to understand the motions of the channel. The addition of modes 9-12 to the analysis did not provide more insight, and the eigenvalues of modes above 12 were significantly lower (*Appendix 4*).

GNM**:**

The three slowest modes of the tetramer give the highest contribution to the overall motion; their fraction contributions add up to 14.6% (*Appendix 4*). The two slowest modes are degenerative with the same eigenvalues. In the first, the pore domains of monomers A and C are mobile but the VSDs of these monomers are immobile; whereas the VSDs of monomers B and A are mobile but their PDs are immobile. In the second mode, a similar behavior was observed for the respective juxtaposed monomer pairs. Nevertheless, the shape of the average of these two modes is the same as that of the third, where all four monomers were observed to be involved in the cooperative motion of the structure. The third mode is the slowest individual mode which incorporates the motion of both the VSD and PD in the same monomer and in all the monomers. The shape of the average of the three slowest modes is similar to the shape of the third alone. The next five modes (4-8), with a total contribution to the overall motion of 7.68%, also hold some functional information. These modes describe motion of substructures within the domains, particularly in the VSD.

Specifically, the three slowest GNM modes suggest that each monomer is composed of 7 rigid elements (Fig. 1b (*red*) and *Appendix 5*) that are connected by 6

hinges (Fig. 1b (*green*) and *Appendix 6*). Three of the hinges were previously shown to be functional (44): M325-L328 between the VSD and PD, I402-V410 in the internal gate and T373-D379 around the selectivity filter (Fig. 1).

Analysis of the next five modes revealed more hinges (*Appendix 7*) including a hinge in the S4 helix, which has been detected in experiments (45). The main hinges identified in all the eight slowest modes are presented in Figure 3.

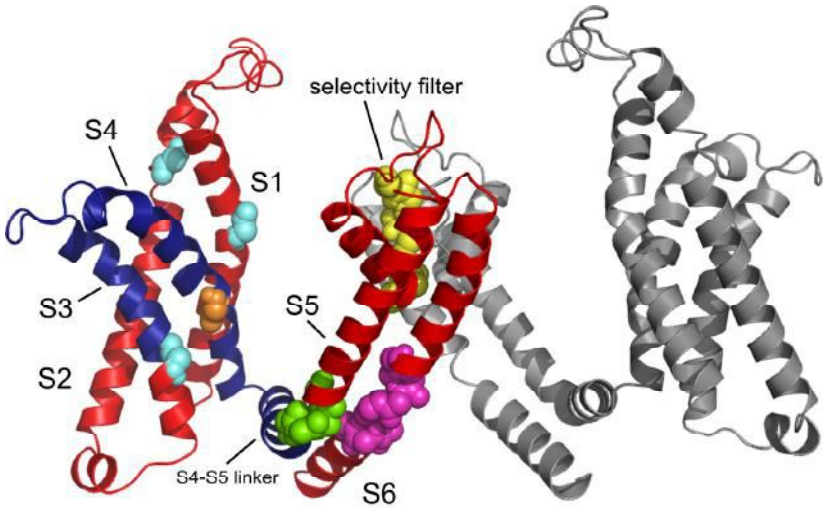

Figure 3: The main hinges as inferred from the eight slowest modes, presented on the 3D model structure of Kv1.2 (7). Only two chains are shown: A in colors and C in gray. The flexible segment, identified in the three slowest modes, containing the S3 and S4 helices, and the S4-S5 linker in chain A are in dark blue. The main chain atoms of the amino acids that were found to serve as hinges are presented as spheres. The hinge in the selectivity filter (T373-D379) is in yellow. The hinge in the S6 helix (I402-V410) is in magenta. The hinge between the S4-S5 linker and the S5 helix (M325-L328) is in green. The hinges in the S1 helix (C181), S2 helix (S217) and S3 helix (V261) are in cyan. These hinges were identified in the first three modes. The hinge in the S4 helix (F302, orange) was identified in the next five modes (4-8). The network of hinges and rigid elements appears to couple between the VSD and PD. The figure was prepared using Pymol (http://www.pymol.org).

ANM:

Comparison of the slowest mode shapes by GNM and ANM allowed us to identify the correspondence between these two elastic models, and thus to predict the direction of the motion controlled by the hinges (*Appendix 8*). The slowest ANM mode describes hinges that are similar to the third GNM mode. The motion of the VSD dominates in this mode and, in comparison, the PD appears to be immobile.

The fourth ANM mode, showing an iris-like motion of the pore (*Appendix 9*), corresponds to the fourth and fifth GNM modes (*Appendix 8*). The same iris-like motion was reported in previous normal mode analysis of various k-channels (33, 34) and recently detected in single molecule experiments (46). It was also shown for the MscL mechanosensitive channel in *E. Coli* (47).

This motion (fourth and fifth GMN modes and fourth ANM mode) is interesting for two reasons. First, it involves all four monomers and represents a coupled motion of the tetramer in order to open and close the channel. Second, it involves coupling between the PDs and VSDs. Thus, it may be associated with gating and the transmission of the voltage sensing to the gates.

b. The correlation between the fluctuations

The hinges can mediate cooperative motions of the rigid elements and the GNM analysis may manifest that. In particular, the analysis may show rigid elements that move in the same and opposite directions with respect to each other.

Identification of motions in groups of slow modes

The average over the eight slowest modes describes the overall motion but not the cooperative fluctuations within the VSD. Therefore we divided these modes into two groups, in accordance with the distribution of their eigenvalues: Modes 1-3 and 4-8. In modes 1-3 (Figs. 4a-4c), the cooperative motions reflected the division of each subunit into two domains: VSD and PD; the main hinge was detected between the S4-S5 linker and S5 helix. In these modes of motion, the VSD behaves as a rigid element. However, the PD is divided into further structural elements by the hinges at the internal gate (the S6 helix) and around the selectivity filter. The PD and the VSD associate through these

flexible regions. In the next five modes (4-8), sub-structural cooperative units appear also in the VSD and the extracellular mouth of the PD (Figs. 4d-4f).

Figure 4 (in the next page): The cooperative motions between residue pairs in the tetramer. The axes mark the residue numbers in each chain. The magnitude of the positive and negative correlations between the fluctuations of the amino acids is color-coded using the red-through-blue scale on the right. (a, d) Interactions within chain A. (b, e) Interactions between residues in chain A and residues in its nearest neighbor (chain B). (c, f) Interactions between residues in chain A and residues in its juxtaposed neighbor (chain C). The different structural segments are marked on the axes.
Panels a-c present averages over the three slowest modes, and panels d-f averages over the next five modes (4-8). Positive correlation indicates a motion of the two residues in the same direction whereas negative correlation indicates a motion in opposite directions.

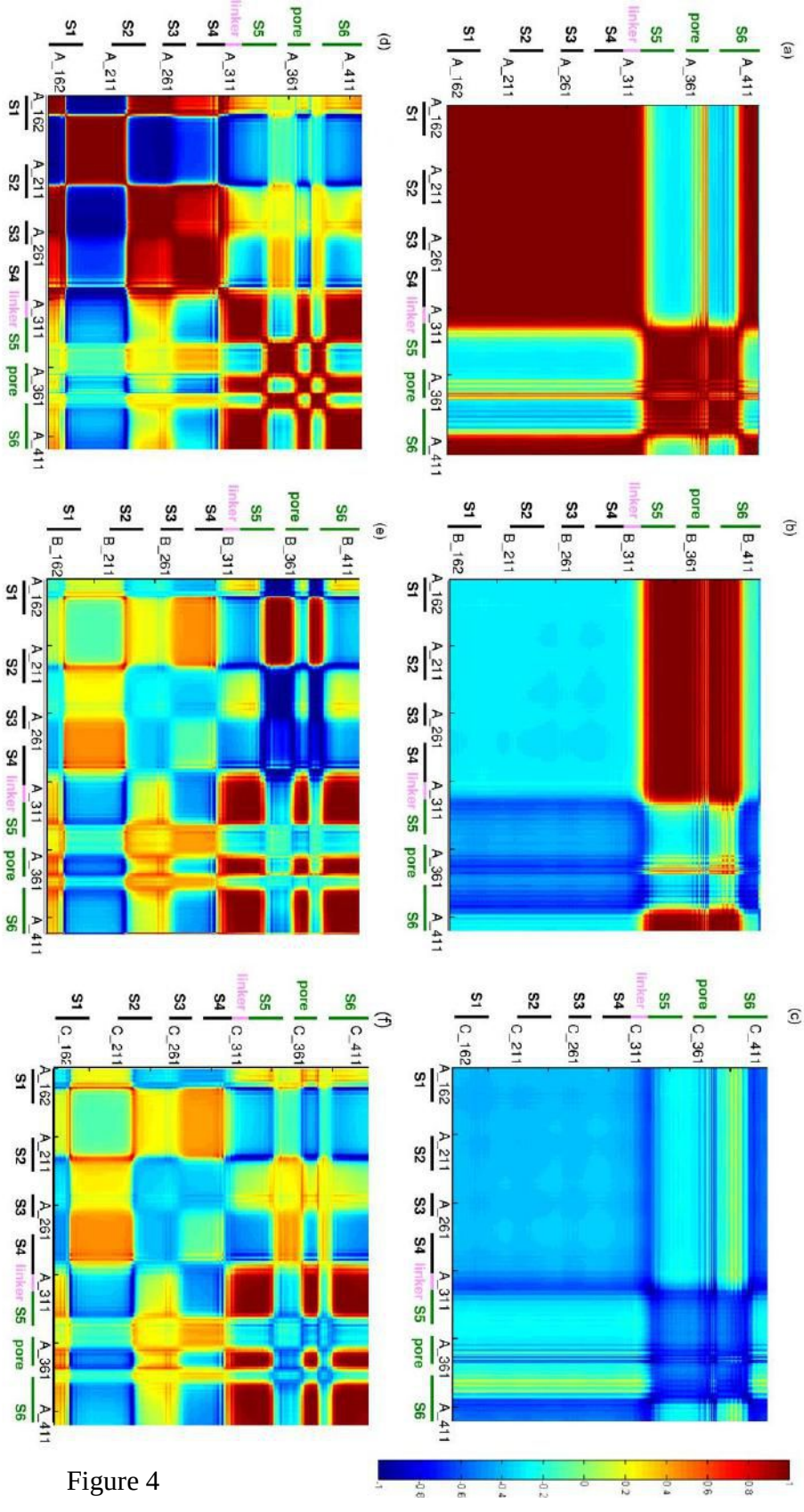
(a)
(b)
(c)
(d)
(e)
(f)
S1
S2
S3
S4
linker
S5
pore
S6
A_162
A_211
A_261
A_311
A_361
A_411
B_162
B_211
B_261
B_311
B_361
B_411
C_162
C_211
C_261
C_311
C_361
C_411
1
0.8
0.6
0.4
0.2
0
-0.2
-0.4
-0.6
-0.8
-1

Figure 4

First, we report the motions of the PD, which have already been identified in previous studies of potassium channels (33, 34, 46, 48-52). Next, we describe the motions of the VSD. We represent the hinges and correlated motions in each domain and between the domains. We show the independent motion of each domain. Last, we show the influence of the VSD on the PD and demonstrate the importance of the tetrameric form of the channel.

The PD

The three slowest modes suggested two hinges in the PD, near the two gates of the channel (Fig. 1, marked as 5 and 6): The first (residues I402-V410) is near the internal gate of the S6 helix, and the second (T373-D379) is in the selectivity filter. The hinge in the S6 helix includes the conserved PVP motif (P405-P407). This hinge allows motion of the C-terminus of the S6 helix, thereby opening and closing of the internal gate. ConSeq analysis (40) revealed that the S6 helix is conserved; especially the PVP motif and the adjacent amino acids (Fig. 2). The T373-D379 segment is also highly conserved.

Complementary analysis of the fastest modes showed that residues T373-D379 of the selectivity filter display high frequency fluctuations (*Appendix 10*), consistent with their being structural hotspots (53). The amino acids in the selectivity filter form the interface between all four monomers. This region has the highest packing density, which limits the mobility of the residues.

The hinge in the selectivity filter is consistent with previously published GNM studies of pore domains from various potassium channels (33, 34). However, the inner helix of KcsA, a potassium channel lacking the VSD, was found to contain two hinges around G99 and L110 (33), instead of one in Kv1.2. These residues are equivalent to G398 and I409 in Kv1.2. In the most cooperative fluctuation modes of Kv1.2 the hinge in the inner helix (S6) appears in I402-V410. The second hinge, around G398, appears in the full tetramer in less cooperative modes (data not shown). A possible explanation for the change between the locations of the hinges may be due to the addition of the VSD in Kv1.2. That is, perhaps the motion of the internal gate in the Kv1.2 structure is limited by

the connection to the large VSD. Supporting the latter, GNM calculations of Kv1.2 in the absence of the VSD resulted in similar hinges to those observed in KcsA.

Several residues are noticed to be important in these regions of the PD. They are highly conserved and associated with various syndromes (*Appendix 11*).

The motion of the internal gate in helix S6 (P407-T421) is positively correlated with the motion of the selectivity filter in each monomer in the three slowest modes (Fig. 4a) as well as in the next five modes (Figs. 4d and *Appendix 12*). The positive correlation indicates that the two rigid elements move in the same direction. This correlation is consistent with experimental studies which showed a correlation between the two gates in the KcsA and *Shaker* channels (48, 51). The correlations between the motions of different parts of the PD (fig. 4) were found to be identical to the correlations in the absence of the VSD (data not shown), which demonstrate the independency of this domain.

The motion of the VSD

I. The hinge between the domains

The three slowest GNM modes suggested that the VSD and PD are connected by a main hinge. The hinge appears between the S4-S5 linker and the S5 helix, around residues M325-L328 (Fig. 1; marked as 4). The sequence analysis identified two conserved residues, E327 and L328, in this region (Fig. 2). E327 of rat Kv1.2 corresponds to E261 in the paralogous Kv7.1 in human. The E261D and E261K mutants of Kv7.1 are associated with Jervell and Lange-Nielsen syndrome (JLNS) and long QT syndrome type 1 (LQT1), respectively (49, 52). Adjacent to this hinge region, S324 is also conserved (Fig. 2). This position, which accommodates only serine, histidine or cysteine, is in the S5 helix, in close proximity to V408 and I409 in the S6 helix. The later positions are also conserved (Fig. 2) and the three residues appear to interact via hydrogen-bonds. The analysis of the corresponding ANM mode also revealed the same region as a hinge (Fig. 5).

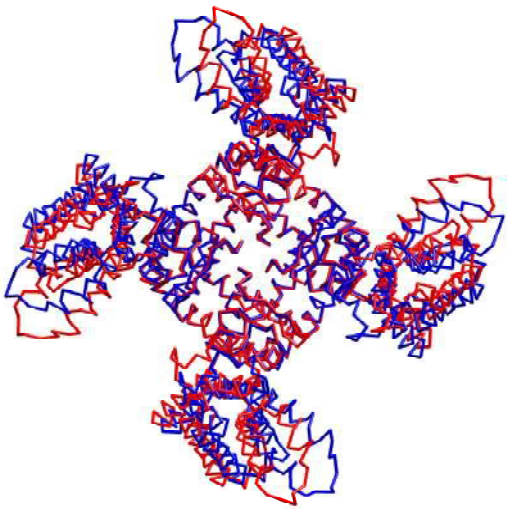

Figure 5: The first ANM mode of fluctuations. The two deformed tetrameric structures, approximately reflecting the motion end-points, are colored blue and red. The original model structure, used for the analysis, is not presented. The positions of the VSDs (periphery) differ between the two structures whereas the PD (center) is, in essence, immobile. The picture was prepared using Pymol (http://www.pymol.org).

Another important observation emerged from the analysis of the same three modes (and the corresponding AMN modes): The S3-S4 paddle (residues A262-V301) and S4-S5 linker (residues S311-S324) move as a rigid unit. This motion appears to be responsible for the mechanical coupling between the VSD and the PD. There are no hinges in the S3-S4 loop, S4 helix and S4-S5 linker (*Appendix 6*): these regions appear to form a rigid structural element that may transmit the motion from the voltage sensor to the pore.

II. The S4 helix

Figure 6 shows the average fluctuations of the three slowest GNM modes, and the fluctuations of the fourth and fifth modes. The S4 helix is a rigid segment in the lowest modes, but a hinge appears in the vicinity of residue F302 in the next two modes (dark and light gray plots; Fig. 6). The hinge is located in the middle of the S4 helix, between R300 and R303, which are highly conserved (Fig. 2) and involved in voltage sensing (10-14). The importance of this hinge has been demonstrated experimentally (45, 54, 55).

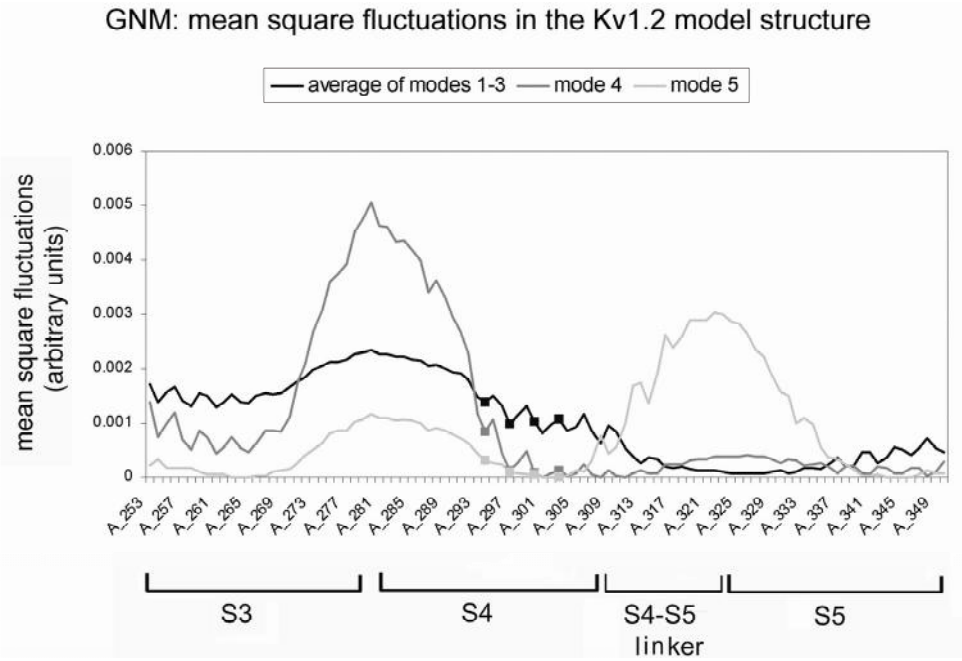

Figure 6**:** Mean square fluctuations of Kv1.2 model structure in the five slowest modes. The averaged mean square fluctuations of modes 1-3 are in black (identical to figure 1a), and the fluctuations of the fourth and fifth modes are in dark and light gray, respectively. The hinge in the S4 helix appears only in the fourth and higher modes, in residue F302. Arginine residues (294, 297, 300 and 303) are marked in squares. Only fluctuations of the S3-S5 helices are presented here, even though the calculation was done for the entire structure. A minimum within the S4 helix appears only from the fourth mode.

III. Other hinges in the VSD

The three hinges in the VSD suggested by the first three GNM modes are around C181 of the S1 helix, S217 of the S2 helix and V261 of the S3 helix (Fig. 1). In the next five modes these hinges shift towards the middle of their respective helices (data not shown). Moreover, in these modes, the same hinges appear to be involved in cooperative motion. Thus, one may envision motion of the helices around the S4 helix. The hinge in the S3 helix is consistent with structural and Biotin-Avidin binding data in the KvAP homologue. The data suggested that the S3 helix is made of two regions: S3a and S3b, and that the S3a helix remains static while the S3b and S4 helices move together when the channel gates (56, 57). The ANM results in the corresponding modes revealed that the S1 and S2 helices move as a rigid unit, in a similar way to the S3-S4 paddle (*Appendix 9*)

Independent motion of the VSD

The calculations for the isolated VSD can demonstrate the modularity of the Kv channels, as elaborated in the rest of this section. Approximately, the hinges that were found to govern the motion of the VSD in the full channel were also found in the isolated VSD. The hinges were found in the vicinity of residues I177 (helix S1), F180 (helix S1), E226 (helix S2), Y266 (helix S3) and R300 (helix S4). The motion of the isolated VSD might thus be sufficient to translate voltage changes into gate closing.

ANM analysis of the isolated VSD revealed several interesting modes of motions. In one mode the identified hinges are located in the middle of the helices. The outer part of the VSD, near the extracellular region, moves clockwise (extracellular view), whereas the inner part, near the intracellular region, moves counterclockwise. This motion reminds the iris-like motion of the whole Kv1.2 tetramer. In another mode the loops between helices S1-S2 and S3-S4 move in different directions. This motion is similar to an opening of a funnel - the extracellular mouth of the VSD opens wider. Both types of motions may help to visualize how the VSD acts as a proton channel.

The dynamic correlations in the isolated VSD were similar to the correlations observed in the VSDs of the whole channel (Appendix 13). The similarity means that the VSD is able to sense the changes in membrane voltage regardless of its coupling to the PD and the other monomers of the channel. This is consistent with recent experiments in the VSOP protein which showed that even though it is expressed as a dimer, the monomer is still functional as a proton channel (58, 59). ANM calculations of the four voltage sensors in the absence of the PDs resulted in independent motion of each VSD. This again implies that the VSDs operate independently.

Correlations and cooperative beaviour

Motion of the tetramer versus motion of the isolated monomer

Voltage sensing is thought to be an independent process for each monomer, and gating is a cooperative motion of the tetrameric form (60-62). To investigate how the cooperativity is reflected by the fluctuations, we compared the GNM mean square fluctuations of the first three modes of the monomer and the first eight modes of the

tetramer (Fig. 7). These appear to approximate the overall behavior in both cases, according to the eigenvalues. The shapes of the average modes are very similar. The hinges in the VSD and PD are identical except for the hinge near R300 of the S4 helix, which appears in a more cooperative mode in the isolated monomer. On the other hand, the hinge between the domains disappeared in the fluctuations of the isolated monomer. The motion of the PD is less restricted in the isolated monomer and thus the C-terminus of the S6 helix appears to be more mobile than in the tetramer.

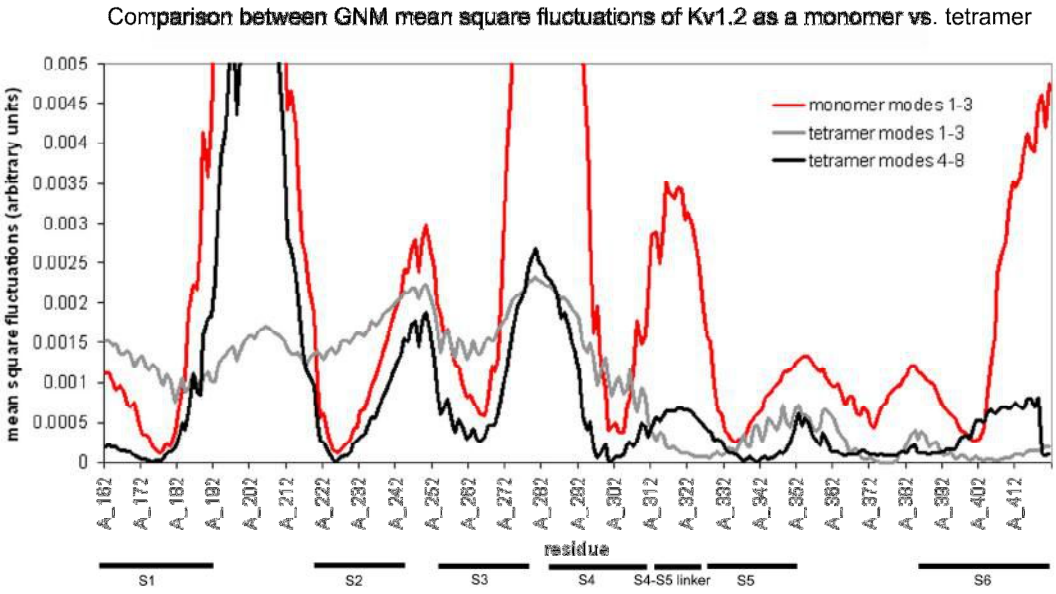

Figure 7: GNM mean square fluctuations of the tetramer and the monomer. The mean square fluctuations of the three slowest modes of the monomer are presented in red. The mean square fluctuations of the three slowest modes of the tetramer are in gray (identical to figure 1a) and the next five modes are in black. The locations of the S1-S6 helices are indicated. Most of the hinges identified in the tetramer appear also in the monomer. The main differences are the higher mobility of S6 and the shift in the location of the hinge between the domains.

The dynamic correlation between the selectivity filter and the VSD within each monomer disappeared in the absence of inter-monomer contacts (Fig. 8b). Moreover, the correlation between the motion of the selectivity filter and the S6 helix is lower, but still positive (Fig. 8b).

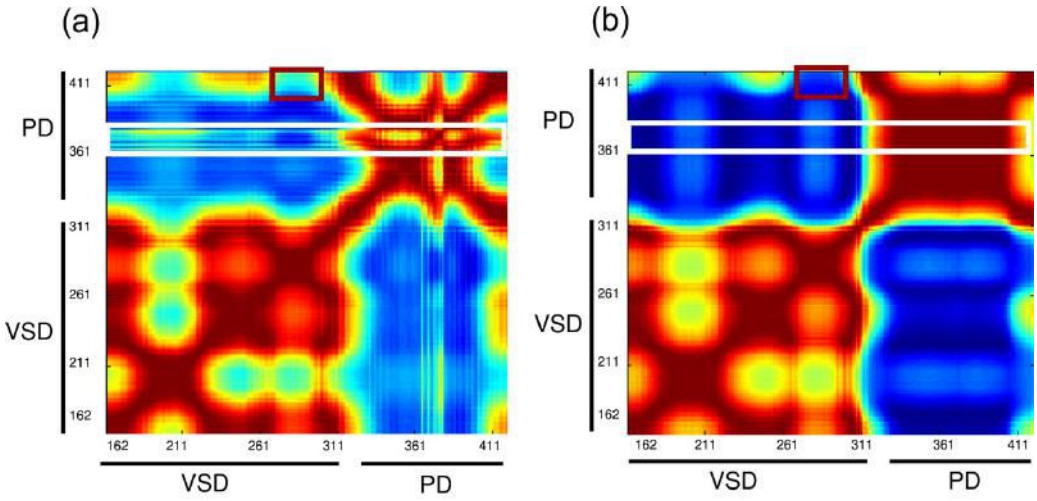

Figure 8: A comparison of correlated fluctuations in an isolated monomer to these of the monomer within the context of the tetramer. (a) Intramolecular cross-correlations of the tetramer (average over modes 1-10). (b) Intramolecular cross-correlations of the isolated monomer (average over modes 1-3). The correlation between the S6 and S4 helices are marked by the brown rectangles. The correlations of the selectivity filter with the rest of the protein are marked by the white rectangles. The color key is the same as in Figure 4. The locations of the domains are marked on the axes. The positive correlation between the selectivity filter and the VSD, observed within the tetramer, disappears in the monomer. The negative correlation between the S6 and S4 helices is higher in the monomer.

To identify the exact interface that causes the changes in motion mentioned above we deleted specific contacts and repeated the calculation. Excluding only the contacts at the interface between the near neighbor monomers led to the appearance of most of the hinges as in the full tetramer but in less cooperative modes. However, the hinge between the domains disappeared in the slowest modes (as well as in the isolated monomer). Excluding the interface between the S4 and S5 helices of each neighboring monomers caused changes in the motions of the S1-S2 and S3-S4 loops in the three slowest modes. The deletion also led to the disappearance of the dynamic correlation between the selectivity filter and the VSD (data not shown). These changes may indicate that the gating motion involves interactions via this interface.

Furthermore, excluding the interface between the selectivity filters of the neighboring monomers also had an effect: The selectivity filter displayed positively correlated fluctuations with the VSD.

Complementary ANM analysis was conducted in search for cooperativity with respect to the direction of the motions. In all slowest ANM modes of the isolated monomer, the selectivity filter moved together with the extracellular regions of the PD as a rigid element. A rotated motion of the S1-S2 and S3-S4 loops was also observed in one of the cooperative modes. This motion reminds the opening of a pore in an iris-like motion of the whole Kv1.2 tetramer. Here the inner parts of the VSD helices, closer to the intracellular part, are less mobile and do not show a counterclockwise motion.

The influence of the sensor on the pore

Correlations between the motion of the gate and the VSD

The analysis of the first three modes suggested that the C-terminal region of the S6 helix (P407-T421), the internal gate, is positively correlated with the whole VSD and selectivity filter in each monomer (Fig. 4a). On the other hand, these regions are negatively correlated with the extracellular regions of the PD (V339-S371, D379-C394). Thus, the internal gate, the selectivity filter, and the VSD behave as elements of the same dynamic unit. The internal gate, is known to be susceptible to depolarization (63, 64). Thus, the observed dynamic correlation between the gate and the VSD may be considered to be functional. Indeed, such functional correlation was found in the human Kv1.5 homologue: The mutation R401N (in the S4 helix) shifted the voltage dependence of activation to negative potentials while the P511G mutation (in the S6 helix) had the opposite effect (65). These positions are equivalent to R297 and P405 in rat Kv1.2, analyzed here.

In the second group of modes, where the hinge inside the S4 helix is visible, the sense of the correlation between the S6 helix and the S3-S4 paddle became negative (Figs. 4d and *Appendix 12*). The coupling between the near neighbor and juxtaposed monomers was negative in all eight slowest modes (Figs. 4b, 4c, 4f and 4e). Nevertheless, the positively correlated fluctuations between these two regions were lost

in the absence of the inter-monomer interactions (Fig. 8b). This implies that the negative intra-monomer coupling of these two regions is intrinsic to the monomer, but the positive intra-monomer coupling requires the interactions between monomers. Thus, the most cooperative modes could be ascribed to the gating process and the next modes are more likely to be associated with the voltage sensing.

A recent sequence analysis detected a group of evolutionarily correlated residues with several positions known to be important for the voltage sensing and gating functions of the channel (Table 1) (66). Some of these positions are located in the paddle (T264, A275 and K277) and internal gate (H418, E420).

Table 1: Evolutionarily correlated positions

KvAP	rKv1.2	Location in 2A79
I18	M171	Helix S1
D20	I173	Helix S1
L103	T264	Helix S3
H109	A275	Loop S3-S4
A111	K277	Loop S3-S4
V240	H418	Helix S6
E242	E420	Helix S6

Evolutionary correlated positions (CorrMut; (66)) in KvAP, the homologous positions in rat Kv1.2 and the locations of these positions in the rat Kv1.2 structure (PDB 2A79).

The fact that amino acids in the internal gate are both evolutionarily (66) and dynamically (here) correlated with amino acids in the S3-S4 paddle helps to reinforce the functional connection between these regions.

This is not the only correlation between the motion of the VSD and the PD: Strong positive inter-monomer correlated fluctuations were detected in the three slowest modes between the S3-S4 paddle and the S5 helix (Fig. 4b- the S3-S4 helices of monomer A and the S5 helix of monomer B). This correlation is negative in the next slowest modes within the monomer and between the monomers (Figs. 4d, 4e and 4f). The negative correlation in the fluctuations of the S3-S4 paddle and S5 helix also holds in the absence of inter-monomer contacts (Fig. 8).

Several mutants in the S4, S5 and S6 helices were shown to change the voltage sensitivity (55, 67, 68). The specific mutations in the S5 and S6 helices are located at the interface between the VSD (the S4 helix) and PD of the near neighbor monomers. The mutations perturbed the equilibrium between the activated and resting states of the sensor, in favor of the resting state (67). A reorientation of the N-terminal region of the S4 helix toward residues in the neighboring PD was shown for Kv1.2 (68). A cooperative gating motion was shown by monitoring the motion of the S4 helix in mutated monomers using environmentally sensitive fluorophore (55). Mutations of residues V369, I372 and S376 in the *Shaker*'s S4 helix to I, L and T, respectively, caused the activation and channel opening to occur over different voltage ranges. Mutating one monomer and comparing its function to a WT channel and a channel in which all monomers are mutated led to the notion that the gating motion of the S4 helix is cooperative (60, 69). The necessity of the inter-monomer connectivity for the correlations between the S3-S4 paddle with the S5 and S6 helices is consistent with the latter experimental studies.

The motion of the S1 helix

Several residues in the C-terminus of the S1 helix were previously shown to be important. For example, T184 is thought to bind E350 of the PD of an adjacent monomer (70). Our results suggest that the N-terminus of the S1 helix is important too. Specifically, it is correlated with the extracellular mouth of the PD, the N-terminus of the S2 helix, the S2-S3 loop, the S3-S4 paddle and the internal part of the S6 helix (Fig. 9). The sense of these correlations changes depending on whether they are located in the same monomer or in different monomers (Figs. 4d-4f). These suggest an interpretation of the correlated substitutions of residues in the S1 helix: I18 and D20 (in KvAP; equivalent to M171 and I173 in rat Kv1.2) (66) with the gate and paddle; the C-terminus of the S1 helix may be involved in gating. Similar analysis of the full Kv1.2 structure, including the intracellular tetramerization domain (T1), revealed similar correlations (data not shown).

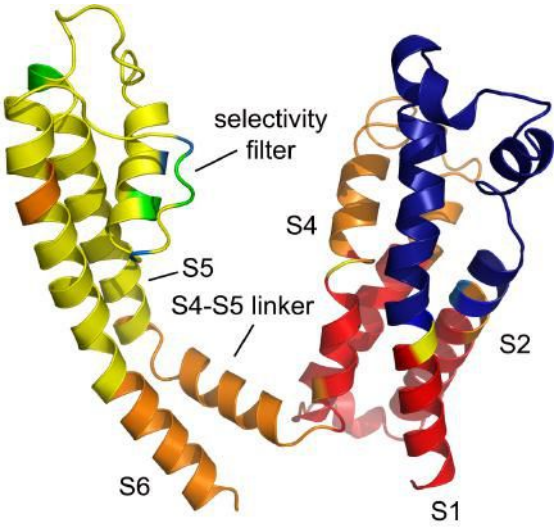

Figure 9: The 3D structure of a monomeric Kv1.2 colored by the cross-correlations between the fluctuations of residues in the N-terminus of the S1 helix and the rest of the monomer, in modes 4-8 (see Figure 4d). The colors key is the same as in Figure 4. Residues of the S1 helix are positively correlated with other functional regions, including the S4 helix and the internal gate in helix S6. The picture was prepared using Pymol (http://www.pymol.org).

Discussion

The dynamics of biomolecular structures are complex and involve various motions, local through global, occurring during a wide range of time scales. Here, within the approximations of the elastic network models, to reflect the intrinsic dynamics of the channel structure, we searched for cooperative modes of motion. The slow fluctuation modes clustered into two groups, each with approximately the same eigenfrequency. Thus, the analysis reflects the dynamics at two different time-scales.

We showed that the two groups of few slow modes are sufficient in order to observe interesting correlations of the dynamic fluctuations between the domains and between the monomers. The first group, representing fluctuations of the longest time scale, includes the three slowest modes. It revealed the hinges that are sufficient to describe the gating motions and some of the internal motions of the VSD. In addition, the fluctuations in these modes presented correlations between the two domains and within the PD (but not the VSD, which moves only as a rigid body). The second group, comprising the next five modes, revealed also a hinge in the S4 helix. Further, the correlated fluctuations in these modes displayed more rigid elements in the VSD and extracellular mouth of the PD.

Overall, the results are consistent with the notion that movement of the charged arginines of the VSD propagates to the outer helix of the PD, thereby opening the pore (56). The network of seven main hinges (Fig. 3) reveals how coupling between the two domains is made possible: The hinge in the internal gate of the S6 helix is located near the hinge in the S4-S5 linker. The S4-S5 linker, on the other hand, forms a rigid unit with the S3-S4 paddle (residues A262-S324; dark blue in Fig. 3). Thus, a motion of the paddle in the membrane may pull the N-terminus of the S5 helix, which is very close to the hinge in the S6 helix. With this, the changes in the packing around the gate hinge may influence the motion of the internal gate. This motion, which was identified in the first group of slow modes, leads us to suggest that these modes are responsible for the gating motion- a motion towards the opening of the gate in the PD. However, the identification of a hinge in the S4 helix in the next group of modes may contribute to defining these modes as activation motions- motions that are associated with the transduction of voltage sensing into conformational changes, ultimately leading to gating.

The motion of the S4 helix, which was observed here, is thought to be responsible for voltage sensing. The appearance of the hinge near the center of the helix in the isolated VSD, the monomer, and the tetramer implies that each voltage sensor has the capacity to function independently. This suggestion is supported by studies of chimeras of Kv2.1 with the paddle from VSOP and Ci-VSP (23). All suggest that the paddle motif is a modular unit which is common to voltage sensors of different proteins. However, some of the motions observed here involve cooperativity in the dynamics of the internal part of the S1 helix and the selectivity filter, suggesting that these regions, which are remote from each other in two different structural domains, are allosterically coupled.

The analysis revealed correlation between the fluctuations of the selectivity filter, located in the external region of the channel, and the internal parts of the PD and VSD. The correlation was observed in both groups of the slowest modes as well as in the average over all eight slowest modes. It indicates a functional connection between the fluctuations of the outer gate (selectivity filter) and the fluctuations of the internal parts of the structure. The selectivity filter and internal gate were also found to be dynamically and evolutionarily correlated (66) with residues in the internal part of the S1 helix. Because these correlations were detected using two complementary computational approaches, it would be interesting to examine them also in experiment.

The motions described here are consistent with gating mechanisms that were previously proposed in that the S3 and S4 helices appear as a rigid structural unit (44). The motion of this unit with respect to the rest of the structure is in accordance with the paddle model of gating (32). It is also consistent with data that showed that the paddle moves as a unit in response to changes in membrane voltage, when tarantula toxins bind the paddle (23).

Monte Carlo simulations predicted a rotation of the S4 helix relative to the S3 helix during the conformational change (7), in contradiction to the paddle model. This suggestion is supported by luminescence resonance energy transfer (LRET) (71) and cystein cross-linking (72) experimets in the *Shaker* channel. We did not detect such motion; perhaps it would have been visible in higher fluctuation modes? In this context it is important to notice that normal mode analysis suffers from a major weakness: One cannot be sure how many modes should be included. We analyzed here eight modes since

the rest were assigned lower eigenvalues (*Appendix 4*), and the analysis appeared to capture the vast majority of biologically relevant motions.

To summarize, we utilized a simple computational model to explore the functional motions of the Kv1.2 channel. In general, the present analysis of the fluctuations revealed the existence of independent and cooperative motions. These are reminiscent of modularity and hierarchical organization of structural units that are plausible for the channel's function. Within this framework, the differences in the hinges and the dynamic couplings observed between the monomer and the tetramer yields a dynamic fingerprint for Kv channels reflected by the fluctuations: The voltage sensing motion occurs independently within each monomer, whereas gating is a cooperative motion of all four monomers.

References

.1 Sanguinetti, M. C., and P. S. Spector. 1997. Potassium channelopathies. Neuropharmacology 36:755-762.

.2 Keblesh, J., D. Hu, and H. Xiong. 2008. Voltage-gated Potassium Channels in Human Immunodeficiency Virus Type-1 (HIV-1)-associated Neurocognitive Disorders. J Neuroimmune Pharmacol. In Press

.3 Koh, K., W. J. Joiner, M. N. Wu, Z. Yue, C. J. Smith, and A. Sehgal. 2008. Identification of SLEEPLESS, a sleep-promoting factor. Science 321:372-376.

.4 Jiang, Y., A. Lee, J. Chen, V. Ruta, M. Cadene ,B. T. Chait, and R. MacKinnon. 2003. X-ray structure of a voltage-dependent K+ channel. Nature 423:33-41.

.5 Long, S. B., E. B. Campbell, and R. Mackinnon. 2005. Crystal structure of a mammalian voltage-dependent Shaker family K+ channel. Science 309:897-903.

.6 Pathak, M. M., V. Yarov-Yarovoy, G. Agarwal, B. Roux, P. Barth, S. Kohout, F. Tombola, and E. Y. Isacoff. 2007. Closing in on the resting state of the Shaker K(+) channel. Neuron 56:124-140.

.7 Yarov-Yarovoy, V., D. Baker, and W. A .Catterall. 2006. Voltage sensor conformations in the open and closed states in ROSETTA structural models of K(+) channels. Proceedings of the National Academy of Sciences of the United States of America 103:7292-7297.

.8 Long, S. B., X. Tao, E. B. Campbell, and R. MacKinnon. 2007. Atomic structure of a voltage-dependent K+ channel in a lipid membrane-like environment. Nature 450:376-382.

.9 Lee, S. Y., A. Lee, J. Chen, and R. MacKinnon. 2005. Structure of the KvAP voltage-dependent K+ channel and its dependence on the lipid membrane. Proceedings of the National Academy of Sciences of the United States of America 102:15441-15446.

.10 Aggarwal, S. K., and R. MacKinnon. 1996. Contribution of the S4 segment to gating charge in the Shaker K+ channel. Neuron 1.6:1169-1177

.11 Ahern, C. A., and R. Horn. 2004. Specificity of charge-carrying residues in the voltage sensor of potassium channels. The Journal of general physiology 123:205-216.

.12 Baker, O. S., H. P. Larsson, L. M. Mannuzzu, and E. Y. Isacoff. 1998 .Three transmembrane conformations and sequence-dependent displacement of the S4 domain in shaker K+ channel gating. Neuron 20:1283-1294.

.13 Seoh, S. A., D. Sigg, D. M. Papazian, and F. Bezanilla. 1996. Voltage-sensing residues in the S2 and S4 segments of the Shaker K+ channel. Neuron 16:1159-1167.

.14 Wang, M. H., S. P. Yusaf, D. J. Elliott, D. Wray, and A. Sivaprasadarao. 1999. Effect of cysteine substitutions on the topology of the S4 segment of the Shaker potassium channel: implications for molecular models of gating. The Journal of physiology 521 Pt 2:315-326.

.15 Starace, D. M., E. Stefani, and F. Bezanilla. 1997. Voltage-dependent proton transport by the voltage sensor of the Shaker K+ channel. Neuron 19:1319-1327.

.16 Tombola, F., M. M. Pathak ,P. Gorostiza, and E. Y. Isacoff. 2007. The twisted ion-permeation pathway of a resting voltage-sensing domain. Nature 445:546-549.
.17 Yang, N., and R. Horn. 1995. Evidence for voltage-dependent S4 movement in sodium channels. Neuron 15:213-218.
.18 Murata, Y., H. Iwasaki, M. Sasaki, K. Inaba, and Y. Okamura. 2005. Phosphoinositide phosphatase activity coupled to an intrinsic voltage sensor. Nature 435:1239-1243.
.19 Hossain, M. I., H. Iwasaki, Y. Okochi, M. Chahine, S. Higashijima, K. Nagayama, and Y. Okamura. 2008. Enzyme domain affects the movement of the voltage sensor in ascidian and zebrafish voltage-sensing phosphatases. The Journal of biological chemistry 283:18248-18259.
.20 Iwasaki, H., Y. Murata, Y. Kim, M. I. Hossain, C. A. Worby, J. E. Dixon ,T. McCormack, T. Sasaki, and Y. Okamura. 2008. A voltage-sensing phosphatase, Ci-VSP, which shares sequence identity with PTEN, dephosphorylates phosphatidylinositol 4,5-bisphosphate. Proceedings of the National Academy of Sciences of the United States of America 105:7970-7975.
.21 Kohout, S. C., M. H. Ulbrich, S. C. Bell, and E. Y. Isacoff. 2008. Subunit organization and functional transitions in Ci-VSP. Nature structural & molecular biology 15:106-108.
.22 Ramsey, I. S., M. M. Moran, J. A. Chong, and D .E. Clapham. 2006. A voltage-gated proton-selective channel lacking the pore domain. Nature 440:1213-1216.
.23 Alabi, A. A., M. I. Bahamonde, H. J. Jung, J. I. Kim, and K. J. Swartz. 2007. Portability of paddle motif function and pharmacology in voltage sensors. Nature 450:370-375.
.24 Chanda, B., O. K. Asamoah, R. Blunck, B. Roux, and F. Bezanilla. 2005. Gating charge displacement in voltage-gated ion channels involves limited transmembrane movement. Nature 436:852-856.
.25 Starace, D. M., and F. Bezanilla. 2004. A proton pore in a potassium channel voltage sensor reveals a focused electric field. Nature 427:548-553.
.26 Bezanilla, F. 2002. Voltage sensor movements. The Journal of general physiology 120:465-473.
.27 Durell, S. R., I. H. Shrivastava, and H. R. Guy. 2004. Models of the structure and voltage-gating mechanism of the shaker K+ channel. Biophysical journal 87:2116-2130.
.28 Ahern, C. A., and R. Horn. 2004. Stirring up controversy with a voltage sensor paddle. Trends in neurosciences 27:303-30.7
.29 Yang, N., A. L. George, Jr., and R. Horn. 1996. Molecular basis of charge movement in voltage-gated sodium channels. Neuron 16:113-122.
.30 Yang, N., A. L. George, Jr., and R. Horn. 1997. Probing the outer vestibule of a sodium channel voltage sensor. Biophysical journal 73:2260-2268.
.31 Goldstein, S. A., L. A. Price, D. N. Rosenthal, and M. H. Pausch. 1996. ORK1, a potassium-selective leak channel with two pore domains cloned from Drosophila melanogaster by expression in Saccharomyces cerevisiae .Proceedings of the National Academy of Sciences of the United States of America 93:13256-13261.

.32 Jiang, Y., V. Ruta, J. Chen, A. Lee, and R. MacKinnon. 2003. The principle of gating charge movement in a voltage-dependent K+ channel. Nature 423:42-48.
.33 Haliloglu, T., and N. Ben-Tal. 2008. Cooperative transition between open and closed conformations in potassium channels. PLoS Comput Biol 4:e1000164.
.34 Shrivastava, I. H., and I. Bahar. 2006. Common mechanism of pore opening shared by five different potassium channels. Biophysical journal 90:3929-3940.
.35 Bahar, I., and A. J. Rader. 2005. Coarse-grained normal mode analysis in structural biology. Current opinion in structural biology 15:586-592.
.36 Haliloglu, T., Bahar I and Erman B. 1997. Gaussian dynamics of folded proteins. Phys. Rev. Lett. 79:3090-3093.
.37 Bahar, I., A. R. Atilgan, and B. Erman. 1997. Direct evaluation of thermal fluctuations in proteins using a single-parameter harmonic potential. Folding & design 2:173-181.
.38 Atilgan, A .R., S. R. Durell, R. L. Jernigan, M. C. Demirel, O. Keskin, and I. Bahar. 2001. Anisotropy of fluctuation dynamics of proteins with an elastic network model. Biophysical journal 80:505-515.
.39 Emekli, U., D. Schneidman-Duhovny, H. J. Wolfson, R. Nussinov ,and T. Haliloglu. 2008. HingeProt: automated prediction of hinges in protein structures. Proteins 70:1219-1227.
.40 Berezin, C., F. Glaser, J. Rosenberg, I. Paz, T. Pupko, P. Fariselli, R. Casadio, and N. Ben-Tal. 2004. ConSeq: the identification of functionally and structurally important residues in protein sequences. Bioinformatics (Oxford, England) 20:1322-1324.
.41 Edgar, R. C. 2004. MUSCLE: multiple sequence alignment with high accuracy and high throughput. Nucleic acids research 32:1792-1797.
.42 Bairoch, A., B. Boeckmann, S. Ferro, and E. Gasteiger. 2004. Swiss-Prot: juggling between evolution and stability. Briefings in bioinformatics 5:39-55.
.43 Mayrose, I., D. Graur, N. Ben-Tal, and T. Pupko. 2004. Comparison of site-specific rate-inference methods for protein sequences: empirical Bayesian methods are superior. Molecular biology and evolution 21:1781-1791.
.44 Tombola, F., M. M. Pathak, and E. Y. Isacoff. 2006. How does voltage open an ion channel? Annual review of cell and developmental biology 22:23-52.
.45 Cuello, L. G., D. M. Cortes, and E. Perozo. 2004. Molecular architecture of the KvAP voltage-dependent K+ channel in a lipid bilayer. Science 306:491-495.
.46 Shimizu, H., M. Iwamoto, T. Konno, A. Nihei, Y. C. Sasaki, and S. Oiki. 2008. Global twisting motion of single molecular KcsA potassium channel upon gating. Cell 132:67-78.
.47 Valadie, H., J. J. Lacapcre, Y. H. Sanejouand, and C. Etchebest. 2003. Dynamical properties of the MscL of Escherichia coli: a normal mode analysis. Journal of molecular biology 332:657-674.
.48 Blunck, R., J. F. Cordero-Morales, L. G. Cuello, E. Perozo, and F. Bezanilla. 2006. Detection of the opening of the bundle crossing in KcsA with fluorescence lifetime spectroscopy reveals the existence of two gates for ion conduction. The Journal of general physiology 128:569-581.
.49 Franqueza, L., M. Lin, J. Shen, I. Splawski, M. T. Keating, and M. C. Sanguinetti. 1999. Long QT syndrome-associated mutations in the S4-S5 linker of KvLQT1

potassium channels modify gating and interaction with minK subunits. The Journal of biological chemistry 274:21063-21070.

.50 Miloshevsky, G. V., and P. C. Jordan. 2007. Open-state conformation of the KcsA K+ channel: Monte Carlo normal mode following simulations. Structure 15:1654-1662.

.51 Yifrach, O., and R. MacKinnon. 2002. Energetics of pore opening in a voltage-gated K(+) channel. Cell 111:231-239.

.52 Tranebjaerg, L., J. Bathen, J. Tyson, and M. Bitner-Glindzicz. 1999. Jervell and Lange-Nielsen syndrome: a Norwegian perspective. American journal of medical genetics 89:137-146.

.53 Demirel, M. C., A. R. Atilgan, R. L. Jernigan, B. Erman, and I. Bahar. 1998. Identification of kinetically hot residues in proteins. Protein Sci 7:2522-2532.

.54 Ledwell, J. L., and R .W. Aldrich. 1999. Mutations in the S4 region isolate the final voltage-dependent cooperative step in potassium channel activation. The Journal of general physiology 113:389-414.

.55 Pathak, M., L. Kurtz, F. Tombola, and E. Isacoff. 2005. The cooperative voltage sensor motion that gates a potassium channel. The Journal of general physiology 125:57-69.

.56 Banerjee, A., and R. MacKinnon. 2008. Inferred motions of the S3a helix during voltage-dependent K+ channel gating. Journal of molecular biology 381:56.9-580

.57 Ruta, V., J. Chen, and R. MacKinnon. 2005. Calibrated measurement of gating-charge arginine displacement in the KvAP voltage-dependent K+ channel. Cell 123:463-475.

.58 Koch, H. P., T. Kurokawa, Y. Okochi, M. Sasaki, Y. Okamura, and H. P. Larsson. 2008. Multimeric nature of voltage-gated proton channels. Proceedings of the National Academy of Sciences of the United States of America. 105 :9111-9116.

.59 Tombola, F., M. H. Ulbrich, and E. Y. Isacoff. 2008. The voltage-gated proton channel Hv1 has two pores, each controlled by one voltage sensor. Neuron 58:546-556.

.60 Schoppa, N. E., and F. J. Sigworth. 1998. Activation of Shaker potassium channels. III. An activation gating model for wild-type and V2 mutant channels. The Journal of general physiology 111:313-342.

.61 Tytgat, J., and P. Hess. 1992. Evidence for cooperative interactions in potassium channel gating. Nature 359:420-423.

.62 Zandany, N., M. Ovadia, I. Orr, and O. Yifrach. 2008. Direct analysis of cooperativity in multisubunit allosteric proteins. Proceedings of the National Academy of Sciences of the United States of America 105:11697-11702.

.63 Choi, K. L., C. Mossman, J. Aube, and G. Yellen. 1993. The internal quaternary ammonium receptor site of Shaker potassium channels. Neuron 10:533-541.

.64 Liu, Y., M. Holmgren, M. E. Jurman, and G. Yellen. 1997. Gated access to the pore of a voltage-dependent K+ channel. Neuron 19:175-184.

.65 Labro, A. J., A. L. Raes, and D. J. Snyders. 2005. Coupling of voltage sensing to channel opening reflects intrasubunit interactions in kv channels. The Journal of general physiology 125:71-80.

.66 Fleishman, S. J., O. Yifrach, and N. Ben-Tal. 2004. An evolutionarily conserved network of amino acids mediates gating in voltage-dependent potassium channels. Journal of molecular biology 340:307-318.
.67 Soler-Llavina, G. J., T. H. Chang, and K. J. Swartz. 2006. Functional interactions at the interface between voltage-sensing and pore domains in the Shaker K(v) channel. Neuron 52:623-634.
.68 Lewis, A., V. Jogini, L. Blachowicz, M. Laine, and B. Roux. 2008. Atomic constraints between the voltage sensor and the pore domain in a voltage-gated K+ channel of known structure. The Journal of general physiology 131:549-561.
.69 Zagotta, W. N., T. Hoshi, and R. W. Aldrich. 1994 .Shaker potassium channel gating. III: Evaluation of kinetic models for activation. The Journal of general physiology 103:321-362.
.70 McKeown, L., M. P. Burnham, C. Hodson, and O. T. Jones. 2008. Identification of an evolutionarily-conserved extracellular threonine residue critical for surface expression and its potential coupling of adjacent voltage-sensing and gating domains in voltage-gated potassium channels. The Journal of biological chemistry. 283:30421-30432.
.71 Posson, D. J., and P. R. Selvin. 2008. Extent of voltage sensor movement during gating of shaker K+ channels. Neuron 59:98-109.
.72 Broomand, A., and F. Elinder. 2008. Large-scale movement within the voltage-sensor paddle of a potassium channel-support for a helical-screw motion. Neuron 59:770-777.
.73 Tombola, F., M. M. Pathak, and E. Y. Isacoff. 2005. Voltage-sensing arginines in a potassium channel permeate and occlude cation-selective pores. Neuron 45:379-388.
.74 Laine, M., M. C. Lin, J. P. Bannister, W. R. Silverman, A. F. Mock, B. Roux, and D. M. Papazian. 2003. Atomic proximity between S4 segment and pore domain in Shaker potassium channels. Neuron 39:467-481.
.75 Jiang, Y., A. Lee, J. Chen, M. Cadene, B. T. Chait, and R. MacKinnon. 2002. Crystal structure and mechanism of a calcium-gated potassium channel. Nature 417:515-522.
.76 Smith, J. A., C. G. Vanoye, A. L. George, Jr., J. Meiler, and C. R. Sanders. 2007. Structural models for the KCNQ1 voltage-gated potassium channel. Biochemistry 46:14141-14152.

Appendix

List of contents

Appendix 1

The PDs of different K-channels are similar VSDs may be different

Several X-ray structures of Kv channels are available. Jiang et al determined the structure of the KvAP channel in its open conformation (4). The protein was crystallized with monoclonal antibodies. The S3-S4 paddles are located near the intracellular membrane surface, perpendicular to the pore axis. Lee et al determined the structure of KvAP in its open conformation (9). In this structure the S3-S4 loop was determined to be outside the membrane, because it was crystallized in a micelle. The protein was crystallized with Fv fragments but the conformation was similar to the crystals without Fv fragments in a lower resolution. Lee et al also created a model structure of KvAP based on the two previous KvAP structures (4, 9) as it would be in a lipid bilayer (9). Long et al determined the structure of the Kv1.2 channel in its open/inactivated state (5). On one hand, the location of the C-terminus of S6 helix is in the open state. On the other hand, two of the S4 arginines are buried in the protein whereas the other two are exposed to the lipid. This state of S4 helix refers to the inactive conformation. Some of the amino acids positions in the loops between the helices of the VSD are missing. Furthermore, the positions of specific residues in S2 and S3 are missing.

Yarov-Yarovoy et al built a model structure of the Kv1.2 channel (7), based on the last structure (4) using the ROSETTA software package. We used their model structure here. They also modeled the closed state using the experimental evidence that E226 in S2 is positioned near R294 in the S4 helix in the closed state (73). The group also modeled the open state of KvAP using the X-ray structure (4) and the closed state of Kv1.2 as a template.

Laine et al created a model structure of the open state of KvAP (74), using the PD from the X-ray structure of MthK, which was determined in its open state (75). The model for interaction between the domains was developed using molecular dynamics simulated annealing procedure. In this model the charged S4 helix is predicted to be located between the PDs from different subunits rather than in the periphery of the protein. Loops between the helices of the sensor domain are not included in this model structure and the helices of the sensor domain are all straight.

Pathak et al created a new ROSETTA model structure of Kv1.2 (6) which is similar to the former model (7), but with different loops. The model was based on the results of fluorescence scan.

Long et al determined the structure of a chimera protein composed of rat Kv1.2 with the S3b-S4 paddle from the rat Kv2.1 (8).

A comparison of these structures has shown that the PD is similar in all structures and the differences are mainly in the sensor domain.

Appendix 2

Dependence of the fluctuation modes on the structure

The majority of the calculations were conducted using the model structure of Kv1.2 in its open state. Nevertheless, the hinges were observed also in other structures of the channel. Various X-ray structures and model structures of voltage gated potassium channels were published (6-9, 74, 76). In all the structures analyzed here the three slowest modes display similar contribution to the overall dynamics of the open model of Kv1.2.

In the three slowest modes of the last KvAP structure ((9), PDB 2A0L) no hinge between the S3 and S4 helices was detected. In the next five modes a hinge near L129 (in the middle of the S4 helix) appeared, in addition to a hinge between the S3a and S3b helices (P99). This implies that the S3b and S4 helices form a rigid element, as in Kv1.2. The hinge in P99 is consistent with the Biotin-Avidin experiments (56). The three slowest modes represent the opening of the pore with hinges in the selectivity filter, M217-G222 (the S6 helix) and T160-F184 (the S5 helix) . In these modes hinges in the end of the S1 helix (T47) and between the S3a and S3b helices (G101) were also detected. Overall, the hinges are consistent with these observed in the Kv1.2 model structure. Other modeled structures of KvAP (7, 9) showed the same motions. Papazian's KvAP model (74) showed different motions. In the three slowest modes of this model structure there are hinges in the S2 helix (F279), the S4 helix (M356), the S5 helix (G406), the selectivity filter (W434-D447) and the S6 helix (L468-T469). The hinges in the S5 and S6 helices are located in the interface between these helices, similar to the hinges in Kv1.2. The hinge in the S4 helix appears in its C-terminus rather than between the arginines as in Kv1.2. Loops between the helices of the sensor are not included in this model and the four helices of the VSD are all straight. Therefore, we cannot expect to have motions similar to the other model structures.

The fluctuations of Yarov-Yarovoy's closed model structure of Kv1.2 (7) were identical to the three slowest modes of the open model structure, which was analyzed here. The exception is that the C-terminus of the S6 helix was less mobile in the closed model.

In the three slowest modes of Pathak's Kv1.2 model structure(6) the hinge in the S2 helix (S217) was missing. The fluctuations of the rest of the protein were identical to Yarov-Yarovoy's Kv1.2 model. This model differs from Yarov-Yarovoy's model only in the loops between the helices of the VSD.

In the three slowest modes of the Kv7.1 model structure (76), which is based on Yarov-Yarovoy's Kv1.2 as a template, hinges of the PD were identical to the hinges in Kv1.2. The hinges in the VSD were different: a hinge between the S1 and S2 helices appeared in the three slowest modes (Q147). In the next mode this hinge disappeared and two hinges in the S1 and S2 helices appeared (L137-S140 and T153 respectively). The hinge in the S3 helix appeared in the middle of the helix (I204), next to the hinge in the S4 helix (I235), which appeared between the arginine residues. Still, the two helices moved as a rigid unit.

In the three slowest GNM modes of the chimera structure of Kv1.2 and Kv2.1 (8), there was another hinge in the loop between helices S1 and S2. This structure differs from Yarov-Yarovoy's Kv1.2 model in the loops between the helices of the VSD.

Appendix 3

Elastic Network Models

We analyzed the Kv1.2 model structure using the Gaussian Network Model (GNM) (36, 37) and Anisotropic Network Model (ANM) (38, 39).

GNM

The protein structure is simplified into alpha-carbon atoms and is treated as a three-dimensional elastic network. The residues within a cut off distance are connected by Hookean springs with a uniform force constant γ. Residues i and j are assumed to display Gaussian fluctuations about their mean positions in the separation $\mathbf{R}_{ij} = |\mathbf{R}_j - \mathbf{R}_i|$, where $\mathbf{R}_i$ and $\mathbf{R}_j$ are the respective position vectors of the ith and jth C_α-atoms.
The correlation between the fluctuations of residues i and j, $\Delta\mathbf{R}_i$ and $\Delta\mathbf{R}_j$ is calculated (36, 37) as follows

$$< \Delta\mathbf{R}_i \Delta\mathbf{R}_j> = (3k_BT/\gamma) [\mathbf{\Gamma}^{-1}]_{ij} = (3k_BT/\gamma) \Sigma_k [\lambda_k^{-1} \mathbf{u}_k \mathbf{u}^T_k]_{ij} \qquad (1)$$

Here $\mathbf{\Gamma}$ is the connectivity matrix (or Kirchhoff) matrix. λ_k is k_{th} eigenvalue of $\mathbf{\Gamma}$ and is representative of the frequency of the kth mode of motion. $\mathbf{u}_k$ is kth eigenvector, k_B is the Boltzmann constant and T is the absolute temperature in degrees Kelvin. This equation provides a way to decompose the dynamics into N-1 eigenmodes for N interacting residues. The contribution of each motion is scaled with the inverse frequency of that mode. The slowest modes thus contribute most to the predicted fluctuations. A few slowest modes were shown to be collective and possibly relevant to the functionality of the biomolecules (35).

The global and local minima points in the fluctuations profiles of each mode are reffered to hinge points. The structural segments which are connected by hinge points form rigid parts.

The dynamic correlations are calculated by the cross- correlations between the fluctuations of each pair of amino acids (36, 37). The correlation between $\Delta\mathbf{R}_i$ and $\Delta\mathbf{R}_j$ is calculated by equation 1, when $i \neq j$. This analysis is used to identify cooperative motions between different segments within the monomer and between the monomers.

Specific pairs of amino acids, in the interfaces between the monomers, were excluded from the calculation in order to identify the region which affects the cooperation in motion.

ANM

Here **Γ** is replaced by Hessian matrix **H** of the second derivative of the intramolecular potential function in eq 1. **H** is 3N x 3N symmetric matrix. The correlation between $\Delta\mathbf{R}_i$ and $\Delta\mathbf{R}_j$ decomposed into 3N-6 modes of motions is then calculated as follows

$$< \Delta\mathbf{R}_i \cdot \Delta\mathbf{R}_j > = (3k_BT/\gamma)\ tr\ [\mathbf{H}^{-1}] = (3k_BT/\gamma)\ \Sigma_k\ tr[\lambda_k^{-1}\ \mathbf{u}_k\ \mathbf{u}^T_k\ ]_{ij} \qquad (2)$$

$tr[\mathbf{H}^{-1}]_{ij}$ is the trace of the ij^{th} submatrix $[\mathbf{H}^{-1}]_{ij}$ of $\mathbf{H}^{-1}$. It refers to the three different components of $\Delta\mathbf{R}_i$ and $\Delta\mathbf{R}_j$; whereas, when i=j, the self correlations between the components $\Delta\mathbf{R}_i$ are obtained. Here the fluctuation vectors allows to construct and explicitly view pairs of alternative conformations sampled by the individual modes, simply by adding the fluctuation vectors $\pm\Delta\mathbf{R}_i$ to the equilibrium position vectors in the respective modes.

Appendix 4

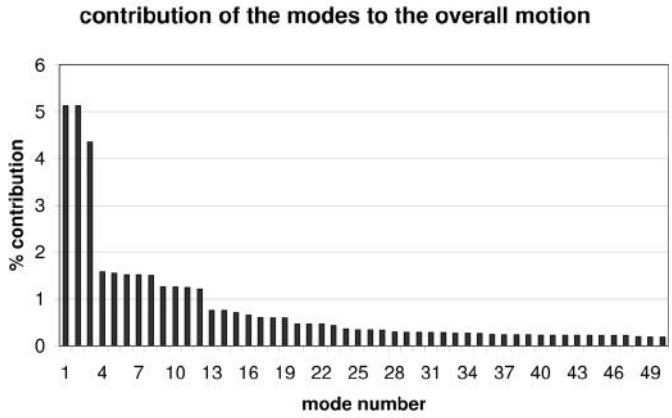

The contribution of the first 50 GNM fluctuation modes to the overall motion of the tetramer. The percentage of contribution is calculated by dividing the frequency of a specific mode by the number of modes. The first three modes have the highest contribution to the overall motion.

Appendix 5

The rigid elements as identified by the first three GNM modes

Residues	**Location in 3D**
A162-C181	The N-terminus of the S1 helix
L182-S217	Loop S1-S2
F218-V261	The S2 helix and the S2-S3 loop
A262-S324	The S3, S4 helices and the S4-S5 linker
G329-M372	The S5 helix and part of the pore loop
M380-T401	The pore loop and the N-terminus of the S6 helix
S411-T421	The C-terminus of the S6 helix

The rigid elements are connected by the hinges which are presented in Appendix 6.

Appendix 6

The hinges as identified by first three GNM modes

Hinge index	Residues	Location in 2A79
1	C181	The S1 helix
2	S217	The S2 helix
3	V261	The S3 helix
4	M325-L328	The S5 helix
5	T373-D379	The selectivity filter
6	I402-V410	The S6 helix

Appendix 7

The hinges as identified by GNM modes 4-8

Hinge index	Residues	Location in 2A79
1	L174-V178	The S1 helix
2	V225	The S2 helix
3	P265	The S3 helix
4	F302	The S4 helix
5	G338-F348	The S5 helix
6	F365	The pore helix
7	T373-N379	The selectivity filter
8	G386-A395	The S6 helix
9	E420	The S6 helix

Appendix 8

Matching GNM and ANM modes

Hinge index	Third GNM mode	First ANM mode	Fifth ANM mode	Fourth GNM mode	Fifth GNM mode	Fourth ANM mode
1	C181	C181	L182	V178	V172-L174	F180
2	S217	C229	T216	F223	W232-S234	T227
3	V261	I254	I254-T269	P265	I264-P265	T269
4	M325-L328	R326	L321	V301	F302-R303	R300
5	T373-D379	T374-V375	T373-G376	L341-F348	S343-V346	A345
6	I402-V410	I402	A403	V390	V381-I389	V390

The hinges in the slowest GNM modes and the corresponding ANM modes, identified by the mean square fluctuations profiles. It is evident that the third GNM mode (which is also similar to the average over modes 1, 2 and 3) corresponds to the first and fifth ANM modes. The fourth ANM mode corresponds to the fourth and fifth GNM modes.

Appendix 9

Two movies of the motion, obtained using ANM, are availabale online at:

http://ibis.tau.ac.il/wiki/nir_bental/index.php/Adva

The motion toward the opening of the pore was inferred by the forth ANM mode. The ANM fluctuations display motion of the cytoplasmic region (red) of the protein in a clockwise direction (from the extracellular side), whereas the other region (blue) moves counterclockwise. The hinges are located in positions F180, T227, T269, R300, A345, V390. (a) A top view from the extracellular side. (b) A side view from the membrane. The motion in this mode shows the opening and closing of the pore together with the motion of the paddle. The movies were generated using PyMol (http://www.pymol.org).

Appendix 10

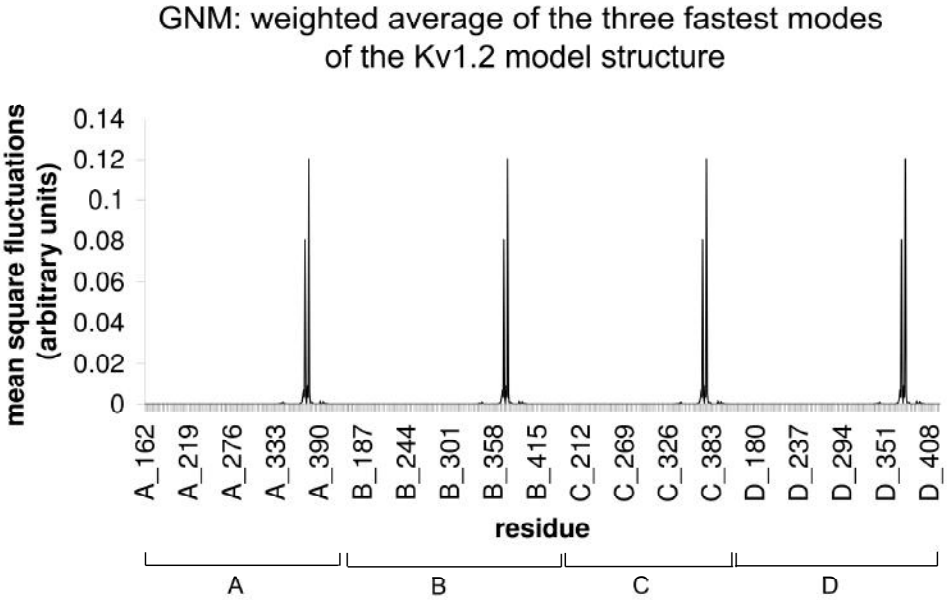

Mean square fluctuations of the three fastest modes. The peaks represent amino acids with high mobility, which means that their motion is fast and restricted. The peaks correspond to positions in the selectivity filter. The chain boundaries are marked on the x-axis.

Appendix 11

Residues near the PD hinges which were found to be important

The three slowest modes suggested two hinges in the PD, near the two gates of the channel: The first (residues I402-V410) is near the internal gate of the S6 helix, and the second (T373-D379) is in the selectivity filter. These hinges allow the opening of the pore. Several residues in these regions were found to be conserved and involved in various syndroms, as elaborated here.

P382, located near the selectivity filter, is highly conserved (Fig. 2). A mutation of the equivalent position in human Kv7.1, a homologous channel that is expressed mainly in the heart and ear, from proline to alanine is associated with long QT syndrome type 1 (LQT1) (52). The side chain of this amino acid points toward G387 (of S6 helix) which is also conserved as glycine.

Adjacent to this hinge region, M372 is also conserved (although a bit less than P382 and G387). This position, which accommodates also leucine or valine, is in close proximity to G338 of the S5 helix and G398 of the S6 helix. A mutation of the corresponding position in Kv7.1 (V310I) also causes LQT1 (52).

Near the selectivity filer, S371 is highly conserved. The only other amino acid in this position in potassium channels is threonine, which is very similar to serine. Na^+ channels contain hydrophobic amino acids in this position (See the MSA in http://ibis.tau.ac.il/wiki/nir_bental/index.php/Adva). S371 is in close proximity to Y377 of the near neighbor monomer. Y377 is part of the GYG motif of the selectivity filter and is highly conserved. The corresponding position in human Kv7.1 is a threonine. Substitution to arginine causes LQT1 in human (52). This mutation may destroy the hydrogen-bond between S/T371 and Y377.

Appendix 12

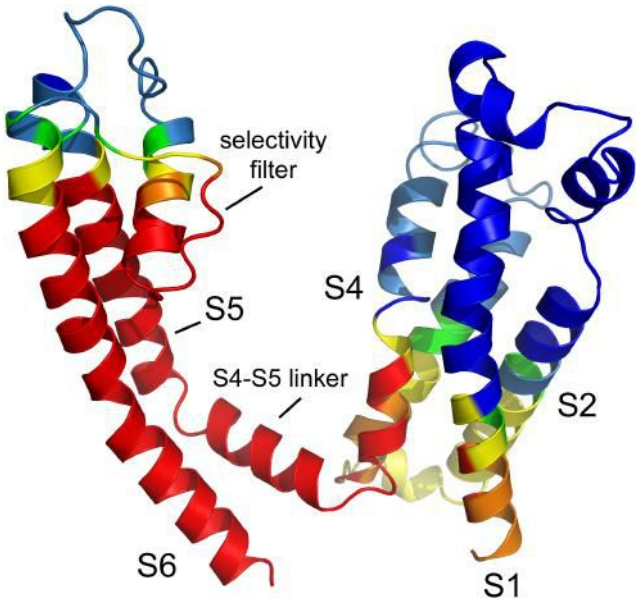

The model structure of a Kv1.2 monomer colored by the cross-correlations between the fluctuations of residues in the C-terminus of the S6 helix and the rest of the monomer, in modes 4-8 (see Figure 4d). The color key is the same as in Figure 4. The motions of the internal gate and the selectivity filter are positively correlated. The figure was prepared using Pymol (http://www.pymol.org).

Appendix 13

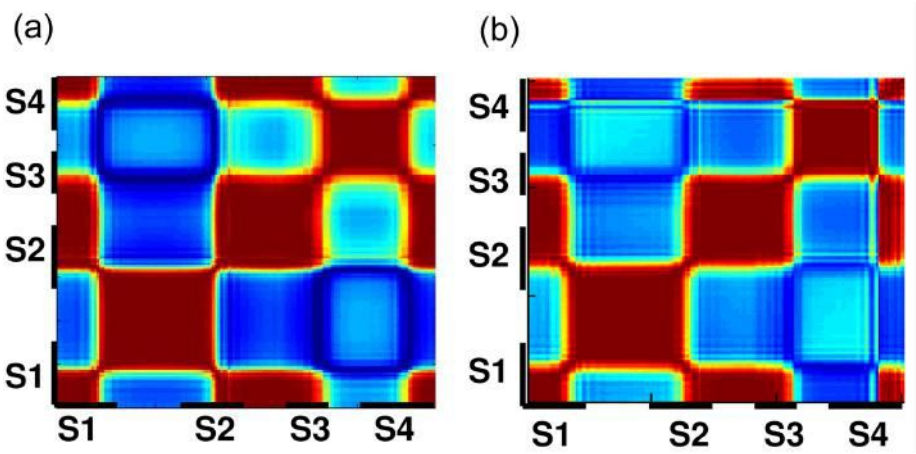

A comparison of correlated fluctuations in an isolated VSD to these of a VSD within the tetramer. (a) Intramolecular cross-correlations of the isolated VSD (average over modes 1-2). (b) Intramolecular cross-correlations of the voltage sensor within the context of the full tetramer (average over modes 4-12). The locations of the S1-S4 helices are marked. The color key is the same as in Figure 4. The correlations within the VSD are very similar, indicating the independet motion of this domain even within the context of the full channel.

תקציר

תעלות אשלגן תלויות מתח, כגון Kv1.2, מעורבות ביצירה והתקדמות של פוטנציאלי פעולה. Kv1.2 מכילה ארבע תת יחידות זהות; כל אחת מהן מורכבת ממתחם חישת המתח (VSD) ומתחם הנקבובית (PD). כדי להעמיק את ההבנה של השינויים הקונפורמציוניים בשני המתחמים אשר מסייעים לפתיחת התעלה וסגירתה, ניתחנו את התנודות של מודל מבני של Kv1.2 באמצעות Gaussian Network Model (GNM) ו- Anisotropic Network Model (ANM). GNM שימש באפיון הצירים והאזורים הקשיחים של המבנה ובצימוד התנועה ביניהם, ו- ANM שימש לחיזוי כיווני התנועה של האזורים הקשיחים. השיטה מאפשרת הצגה של התנועה הכוללת כסכום של אופני-תנודה בדידים. לעיתים קרובות ניתן לקשר בין המצבים האיטיים ביותר לתפקידים ביולוגיים. תנועות חישת המתח ופתיחת השער תוארו כאן באמצעות שתי קבוצות של מצבים. מניתוח התוצאות עולה רשת של תנודות מצומדות של שמונה יחידות מבניות קשיחות המתואמות ע"י שבעה צירים. הרשת מורכבת ברובה מחומצות אמינו הידועות כמעורבות בשינויי הקונפורמציה הקשורים במעבר בין המצב הפעיל ללא פעיל של התעלה, ו/או רגישות לשינויים גנטיים. מן התוצאות עולה צימוד בין התנועה של ה- VSD והפילטר הבורר אשר ב-PD, בהתאמה למידע ניסיוני עדכני. הצימוד, אשר מרמז ליחס תפקודי בין שני האזורים המרוחקים הללו, לא נצפה בתת היחידה הבודדת, מה שמבליט את טבעו האלוסטרי. נקודות מגע ישירות בין מתחמי חישת המתח של ארבע תת היחידות אינן קיימות, והקשרים ביניהם למתחמי התעלה הינם רפויים, מה שרומז ליכולת פעולה עצמאית של כל דומיין. הדומיינים אכן מפגינים הרבה תנודות אינהרנטיות אשר אינן מצומדות ליתר החלבון. באופן כללי ניתוח התוצאות מציע כי שני המתחמים תורמים לתפקוד התעלה גם באופן עצמאי וגם באופן משותף.

אוניברסיטת תל-אביב

הפקולטה למדעי החיים ע"ש ג'ורג' ס. וייז

המדרשה לתארים מתקדמים

תנועות משותפות ועצמאיות של התעלה Kv1.2: חישת מתח ופתיחת השער

חיבור זה הוגש כעבודת גמר לקראת התואר "מוסמך אוניברסיטה"
במסלול ביוכימיה באוניברסיטת תל-אביב

על-ידי

אדוה יחזקאל

העבודה הוכנה במחלקה לביוכימיה של אוניברסיטת תל-אביב

בהנחיית

פרופ' ניר בן-טל

חתימת המנחה:.....

תאריך: ינואר 2009

אוניברסיטת תל-אביב

הפקולטה למדעי החיים ע"ש ג'ורג' ס. וייז

המדרשה לתארים מתקדמים

תנועות משותפות ועצמאיות של התעלה Kv1.2: חישת מתח ופתיחת השער

חיבור זה הוגש כעבודת גמר לקראת התואר "מוסמך אוניברסיטה"
במסלול ביוכימיה באוניברסיטת תל-אביב

על-ידי

אדוה יחזקאל

העבודה הוכנה במחלקה לביוכימיה של אוניברסיטת תל-אביב

בהנחיית

פרופ' ניר בן-טל

תאריך: ינואר 2009